

***Fermi* Large Area Telescope observations of PSR J1836+5925**

A. A. Abdo^{2,3}, M. Ackermann⁴, M. Ajello⁴, W. B. Atwood⁵, L. Baldini⁶, J. Ballet⁷,
 G. Barbiellini^{8,9}, M. G. Baring¹⁰, D. Bastieri^{11,12}, K. Bechtol⁴, A. Belfiore¹³, R. Bellazzini⁶,
 B. Berenji⁴, R. D. Blandford⁴, E. D. Bloom⁴, E. Bonamente^{14,15}, A. W. Borgland⁴, J. Bregeon⁶,
 A. Brez⁶, M. Brigida^{16,17}, P. Bruel¹⁸, T. H. Burnett¹⁹, S. Buson¹², G. A. Caliandro²⁰,
 R. A. Cameron⁴, F. Camilo²¹, P. A. Caraveo¹³, S. Carrigan¹², J. M. Casandjian⁷, C. Cecchi^{14,15},
 Ö. Çelik^{22,23,24}, E. Charles⁴, A. Chekhtman^{2,25}, C. C. Cheung^{2,3}, J. Chiang⁴, S. Ciprini¹⁵,
 R. Claus⁴, J. Cohen-Tanugi²⁶, J. Conrad^{27,28,29}, A. de Angelis³⁰, A. de Luca³¹, F. de Palma^{16,17},
 S. W. Digel⁴, M. Dormody⁵, E. do Couto e Silva⁴, P. S. Drell⁴, R. Dubois⁴, D. Dumora^{32,33},
 Y. Edmonds⁴, C. Farnier²⁶, C. Favuzzi^{16,17}, S. J. Fegan¹⁸, W. B. Focke⁴, P. Fortin¹⁸, M. Frailis³⁰,
 Y. Fukazawa³⁴, S. Funk⁴, P. Fusco^{16,17}, F. Gargano¹⁷, D. Gasparrini³⁵, N. Gehrels^{22,36,37},
 S. Germani^{14,15}, G. Giavitto^{8,9}, N. Giglietto^{16,17}, F. Giordano^{16,17}, T. Glanzman⁴, G. Godfrey⁴,
 I. A. Grenier⁷, M.-H. Grondin^{32,33}, J. E. Grove², L. Guillemot³⁸, S. Guiriec³⁹, C. Gwon²,
 D. Hadasch⁴⁰, A. K. Harding²², E. Hays²², D. Horan¹⁸, R. E. Hughes⁴¹, M. S. Jackson^{28,42},
 G. Jóhannesson⁴, A. S. Johnson⁴, R. P. Johnson⁵, T. J. Johnson^{22,37}, W. N. Johnson²,
 T. Kamae⁴, Y. Kanai⁴³, H. Katagiri³⁴, J. Kataoka⁴⁴, N. Kawai^{43,45,1}, M. Kerr¹⁹, J. Knödlseeder⁴⁶,
 M. Kuss⁶, J. Lande⁴, L. Latronico⁶, M. Lemoine-Goumard^{32,33}, F. Longo^{8,9}, F. Loparco^{16,17},
 B. Lott^{32,33}, M. N. Lovellette², P. Lubrano^{14,15}, G. M. Madejski⁴, A. Makeev^{2,25}, M. Marelli¹³,
 M. N. Mazziotta¹⁷, J. E. McEnery^{22,37}, C. Meurer^{27,28}, P. F. Michelson⁴, W. Mitthumsiri⁴,
 T. Mizuno³⁴, A. A. Moiseev^{23,37}, C. Monte^{16,17}, M. E. Monzani⁴, A. Morselli⁴⁷,
 I. V. Moskalenko⁴, S. Murgia⁴, P. L. Nolan⁴, J. P. Norris⁴⁸, E. Nuss²⁶, T. Ohsugi³⁴, N. Omodei⁶,
 E. Orlando⁴⁹, J. F. Ormes⁴⁸, D. Paneque⁴, J. H. Panetta⁴, D. Parent^{32,33}, V. Pelassa²⁶,
 M. Pepe^{14,15}, M. Pesce-Rollins⁶, M. Pierbattista⁷, F. Piron²⁶, T. A. Porter⁵, S. Rainò^{16,17},
 R. Rando^{11,12}, S. M. Ransom⁵⁰, P. S. Ray², M. Razzano⁶, N. Rea^{20,51}, A. Reimer^{52,4},
 O. Reimer^{52,4,1}, T. Reposeur^{32,33}, L. S. Rochester⁴, A. Y. Rodriguez²⁰, R. W. Romani⁴,
 M. Roth¹⁹, F. Ryde^{42,28}, H. F.-W. Sadrozinski⁵, A. Sander⁴¹, P. M. Saz Parkinson^{5,1},
 J. D. Scargle⁵³, C. Sgrò⁶, E. J. Siskind⁵⁴, D. A. Smith^{32,33}, P. D. Smith⁴¹, G. Spandre⁶,
 P. Spinelli^{16,17}, M. S. Strickman², D. J. Suson⁵⁵, H. Takahashi³⁴, T. Tanaka⁴, J. B. Thayer⁴,
 J. G. Thayer⁴, D. J. Thompson²², S. E. Thorsett⁵, L. Tibaldo^{11,12,7}, O. Tibolla⁵⁶,
 D. F. Torres^{40,20}, G. Tosti^{14,15}, A. Tramacere^{4,57}, T. L. Usher⁴, A. Van Etten⁴, V. Vasileiou^{23,24},
 C. Venter^{22,58}, N. Vilchez⁴⁶, V. Vitale^{47,59}, A. P. Waite⁴, P. Wang⁴, K. Watters⁴, B. L. Winer⁴¹,
 M. T. Wolff², K. S. Wood², T. Ylinen^{42,60,28}, M. Ziegler⁵

¹Corresponding authors: N. Kawai, nkawai@phys.titech.ac.jp; O. Reimer, olr@slac.stanford.edu; P. M. Saz Parkinson, pablo@scipp.ucsc.edu.

²Space Science Division, Naval Research Laboratory, Washington, DC 20375, USA

³National Research Council Research Associate, National Academy of Sciences, Washington, DC 20001, USA

⁴W. W. Hansen Experimental Physics Laboratory, Kavli Institute for Particle Astrophysics and Cosmology, Department of Physics and SLAC National Accelerator Laboratory, Stanford University, Stanford, CA 94305, USA

⁵Santa Cruz Institute for Particle Physics, Department of Physics and Department of Astronomy and Astrophysics, University of California at Santa Cruz, Santa Cruz, CA 95064, USA

⁶Istituto Nazionale di Fisica Nucleare, Sezione di Pisa, I-56127 Pisa, Italy

⁷Laboratoire AIM, CEA-IRFU/CNRS/Université Paris Diderot, Service d'Astrophysique, CEA Saclay, 91191 Gif sur Yvette, France

⁸Istituto Nazionale di Fisica Nucleare, Sezione di Trieste, I-34127 Trieste, Italy

⁹Dipartimento di Fisica, Università di Trieste, I-34127 Trieste, Italy

¹⁰Rice University, Department of Physics and Astronomy, MS-108, P. O. Box 1892, Houston, TX 77251, USA

¹¹Istituto Nazionale di Fisica Nucleare, Sezione di Padova, I-35131 Padova, Italy

¹²Dipartimento di Fisica “G. Galilei”, Università di Padova, I-35131 Padova, Italy

¹³INAF-Istituto di Astrofisica Spaziale e Fisica Cosmica, I-20133 Milano, Italy

¹⁴Istituto Nazionale di Fisica Nucleare, Sezione di Perugia, I-06123 Perugia, Italy

¹⁵Dipartimento di Fisica, Università degli Studi di Perugia, I-06123 Perugia, Italy

¹⁶Dipartimento di Fisica “M. Merlin” dell'Università e del Politecnico di Bari, I-70126 Bari, Italy

¹⁷Istituto Nazionale di Fisica Nucleare, Sezione di Bari, 70126 Bari, Italy

¹⁸Laboratoire Leprince-Ringuet, École polytechnique, CNRS/IN2P3, Palaiseau, France

¹⁹Department of Physics, University of Washington, Seattle, WA 98195-1560, USA

²⁰Institut de Ciències de l'Espai (IEEC-CSIC), Campus UAB, 08193 Barcelona, Spain

²¹Columbia Astrophysics Laboratory, Columbia University, New York, NY 10027, USA

²²NASA Goddard Space Flight Center, Greenbelt, MD 20771, USA

²³Center for Research and Exploration in Space Science and Technology (CRESST) and NASA Goddard Space Flight Center, Greenbelt, MD 20771, USA

²⁴Department of Physics and Center for Space Sciences and Technology, University of Maryland Baltimore County, Baltimore, MD 21250, USA

²⁵George Mason University, Fairfax, VA 22030, USA

²⁶Laboratoire de Physique Théorique et Astroparticules, Université Montpellier 2, CNRS/IN2P3, Montpellier, France

²⁷Department of Physics, Stockholm University, AlbaNova, SE-106 91 Stockholm, Sweden

²⁸The Oskar Klein Centre for Cosmoparticle Physics, AlbaNova, SE-106 91 Stockholm, Sweden

-
- ²⁹Royal Swedish Academy of Sciences Research Fellow, funded by a grant from the K. A. Wallenberg Foundation
- ³⁰Dipartimento di Fisica, Università di Udine and Istituto Nazionale di Fisica Nucleare, Sezione di Trieste, Gruppo Collegato di Udine, I-33100 Udine, Italy
- ³¹Istituto Universitario di Studi Superiori (IUSS), I-27100 Pavia, Italy
- ³²Université de Bordeaux, Centre d’Études Nucléaires Bordeaux Gradignan, UMR 5797, Gradignan, 33175, France
- ³³CNRS/IN2P3, Centre d’Études Nucléaires Bordeaux Gradignan, UMR 5797, Gradignan, 33175, France
- ³⁴Department of Physical Sciences, Hiroshima University, Higashi-Hiroshima, Hiroshima 739-8526, Japan
- ³⁵Agenzia Spaziale Italiana (ASI) Science Data Center, I-00044 Frascati (Roma), Italy
- ³⁶Department of Astronomy and Astrophysics, Pennsylvania State University, University Park, PA 16802, USA
- ³⁷Department of Physics and Department of Astronomy, University of Maryland, College Park, MD 20742, USA
- ³⁸Max-Planck-Institut für Radioastronomie, Auf dem Hügel 69, 53121 Bonn, Germany
- ³⁹Center for Space Plasma and Aeronomic Research (CSPAR), University of Alabama in Huntsville, Huntsville, AL 35899, USA
- ⁴⁰Institució Catalana de Recerca i Estudis Avançats (ICREA), Barcelona, Spain
- ⁴¹Department of Physics, Center for Cosmology and Astro-Particle Physics, The Ohio State University, Columbus, OH 43210, USA
- ⁴²Department of Physics, Royal Institute of Technology (KTH), AlbaNova, SE-106 91 Stockholm, Sweden
- ⁴³Department of Physics, Tokyo Institute of Technology, Meguro City, Tokyo 152-8551, Japan
- ⁴⁴Waseda University, 1-104 Totsukamachi, Shinjuku-ku, Tokyo, 169-8050, Japan
- ⁴⁵Cosmic Radiation Laboratory, Institute of Physical and Chemical Research (RIKEN), Wako, Saitama 351-0198, Japan
- ⁴⁶Centre d’Étude Spatiale des Rayonnements, CNRS/UPS, BP 44346, F-30128 Toulouse Cedex 4, France
- ⁴⁷Istituto Nazionale di Fisica Nucleare, Sezione di Roma “Tor Vergata”, I-00133 Roma, Italy
- ⁴⁸Department of Physics and Astronomy, University of Denver, Denver, CO 80208, USA
- ⁴⁹Max-Planck Institut für extraterrestrische Physik, 85748 Garching, Germany
- ⁵⁰National Radio Astronomy Observatory (NRAO), Charlottesville, VA 22903, USA
- ⁵¹Sterrenkundig Instituut “Anton Pannekoek”, 1098 SJ Amsterdam, Netherlands
- ⁵²Institut für Astro- und Teilchenphysik and Institut für Theoretische Physik, Leopold-Franzens-Universität Innsbruck, A-6020 Innsbruck, Austria
- ⁵³Space Sciences Division, NASA Ames Research Center, Moffett Field, CA 94035-1000, USA
- ⁵⁴NYCB Real-Time Computing Inc., Lattingtown, NY 11560-1025, USA
- ⁵⁵Department of Chemistry and Physics, Purdue University Calumet, Hammond, IN 46323-2094, USA
- ⁵⁶Max-Planck-Institut für Kernphysik, D-69029 Heidelberg, Germany
- ⁵⁷Consorzio Interuniversitario per la Fisica Spaziale (CIFS), I-10133 Torino, Italy
- ⁵⁸North-West University, Potchefstroom Campus, Potchefstroom 2520, South Africa

ABSTRACT

The discovery of the γ -ray pulsar PSR J1836+5925, powering the formerly unidentified EGRET source 3EG J1835+5918, was one of the early accomplishments of the *Fermi* Large Area Telescope (LAT). Sitting 25° off the Galactic plane, PSR J1836+5925 is a 173 ms pulsar with a characteristic age of 1.8 million years, a spindown luminosity of 1.1×10^{34} erg s $^{-1}$, and a large off-peak emission component, making it quite unusual among the known γ -ray pulsar population. We present an analysis of one year of LAT data, including an updated timing solution, detailed spectral results and a long-term light curve showing no indication of variability. No evidence for a surrounding pulsar wind nebula is seen and the spectral characteristics of the off-peak emission indicate it is likely magnetospheric. Analysis of recent *XMM-Newton* observations of the X-ray counterpart yields a detailed characterization of its spectrum, which, like Geminga, is consistent with that of a neutron star showing evidence for both magnetospheric and thermal emission.

Subject headings: gamma rays: general; pulsars: general; pulsars: individual (PSR J1836+5925)

1. Introduction

Since its discovery by EGRET (Lin et al. 1992), the bright high-energy γ -ray source GRO J1837+59 defied straightforward identification. It was reported as a persistent source with a varying flux of $3\text{--}8 \times 10^{-7}$ ph cm $^{-2}$ s $^{-1}$ and a relatively hard spectrum of photon index 1.7 in non-consecutive, typically 2–3 week-long, observing periods. Its location at high Galactic latitude in conjunction with early reports of γ -ray variability (later questioned by Nolan et al. 1996; Reimer et al. 2001) suggested it might be a blazar. However, the lack of a radio-bright counterpart, common to EGRET-detected blazars, cast doubts on such an interpretation.

With the detection of faint X-ray counterpart candidates in the error contour of 3EG J1835+5918 (Reimer et al. 2000), the interpretation focused increasingly on a nearby radio-quiet neutron star. The complete characterization of all but one of the *ROSAT HRI* X-ray sources was presented by Mirabal et al. (2000) and Reimer et al. (2001), who singled out RX J1836.2+5925 as the most probable counterpart of 3EG J1835+5918. Subaru/FOCAS observations in the B- and U-bands proposed possible optical counterparts (Totani et al. 2002), while *Hubble Space Telescope* observations set an optical upper limit of $V > 28.5$ (Halpern et al. 2002). A scenario of a thermally emitting neutron star which was either older or more distant than the archetypal radio-quiet γ -ray pulsar Geminga emerged

⁵⁹Dipartimento di Fisica, Università di Roma “Tor Vergata”, I-00133 Roma, Italy

⁶⁰School of Pure and Applied Natural Sciences, University of Kalmar, SE-391 82 Kalmar, Sweden

as the most plausible explanation for the source (Halpern & Ruderman 1993; Bignami & Caraveo 1996; Mirabal & Halpern 2001), with an upper limit on the distance of 800 pc, determined from X-ray observations (Halpern et al. 2002). Using *Chandra* observations separated by three years, Halpern et al. (2007) were also able to determine an upper limit on the proper motion of $0.14''$ per year, or $v_t < 530 \text{ km s}^{-1}$ at 800 pc. However, a timing signature, which would settle the nature of this source, was never found in the EGRET data (Chandler et al. 2001; Ziegler et al. 2008), nor in repeated observations by *Chandra* (Halpern et al. 2002, 2007), nor in a 24-hr observation with NRAO’s Green Bank Telescope (GBT) (Halpern et al. 2007). Upper limits from Very High Energy (VHE) γ -ray observations (Fegan & Weekes 2005) determined that the peak of emission must be at GeV gamma rays. Recently, AGILE reported marginal flux variability in their 2007–2008 data, arising from several non-detections in a period of long uninterrupted coverage, along with a flux level significantly lower than what was previously reported by EGRET (Bulgarelli et al. 2008).

3EG J1835+5918 was a target of pointed observations during the 60-day commissioning period prior to the start of normal science operations of the Large Area Telescope (LAT) aboard the *Fermi Gamma-ray Space Telescope*. During these observations, the LAT accumulated photons from this source at a rate approximately twice as high as during regular survey-mode operations, thus facilitating the detection of γ -ray pulsations. The discovery and initial timing of the pulsar, PSR J1836+5925, using the first five months of LAT data, were reported in Abdo et al. (2009a). Here we present the phenomenology emerging from one year of LAT observations of PSR J1836+5925, including energy-dependent pulse profiles and phase-resolved spectroscopy.

2. Gamma-ray observations and data analysis

The LAT is a pair conversion telescope, sensitive to gamma rays with energies from 20 MeV to $>300 \text{ GeV}$. Gamma rays in the LAT are recorded with an accuracy of $< 1 \mu\text{s}$. The LAT has an on-axis effective area of 8000 cm^2 , a field of view of $\sim 2.4 \text{ sr}$, and an angular resolution of $\sim 0.8^\circ$ 68% containment at 1 GeV (Atwood et al. 2009).

2.1. Timing analysis

We have derived a precise timing solution of PSR J1836+5925 using data from 2008 June 30 to 2009 June 30 (MJD 54647.4–55013.0). We selected photons with $E > 170 \text{ MeV}$ offset from the source direction by no more than 1.6° , a radius chosen to maximize the pulsed significance, and used the LAT Science Tool¹ `gtbary` in its geocenter mode to correct the arrival times to terrestrial time (TT) at the geocenter. We generated a total of 22 pulse times of arrival (TOAs), each covering roughly two weeks of data, and obtained pulse profiles by folding the photon times according to

¹available at <http://fermi.gsfc.nasa.gov/ssc/data/analysis/>

a provisional ephemeris using polynomial coefficients generated by TEMPO2 (Hobbs et al. 2006) in its predictive mode (assuming a fictitious observatory at the geocenter). The TOAs were then measured by cross correlating each pulse profile with a template consisting of two gaussians, derived from the data set above (Ray et al. 2010). The timing model, fit using TEMPO2, included position, frequency (ν), and frequency derivative ($\dot{\nu}$). Table 1 lists the results of our fit. The 1.3 ms RMS residual to the fit is comparable to the mean TOA measurement uncertainty of 1.2 ms and significantly smaller than the 5.4 ms resolution of our 32 bin light curve. The reduced χ^2 of our timing fit is 1.9. With $\nu = 5.77$ Hz and $\dot{\nu} = -5 \times 10^{-14}$ Hz s $^{-1}$, we derive a characteristic age of 1.8 million years and a spindown luminosity of 10^{34} erg s $^{-1}$. Our best fit location is RA=18:36:13.75(3), Dec=+59:25:30.3(6), which is $0.35''$ from RX J1836.2+5925, well within the statistical uncertainty of the timing fit, securing the association between PSR J1836+5925 and RX J1836.2+5925.

2.2. Light curve

We explored the pulsar light curve in different energy bands by selecting events with energies above 100 MeV from an energy-dependent region of interest (ROI), defined as $\theta = 3.4^\circ (E/100\text{MeV})^{-0.75}$ with a minimum (maximum) radius of 0.35° (2.1°). The rotation phase of each event is calculated using the truncated Taylor series expansion: $\phi = \phi_0 + \nu(t - T_0) + \frac{1}{2}\dot{\nu}(t - T_0)^2$, where T_0 is the reference epoch of MJD 54800 and ϕ_0 is the reference phase at T_0 , which we define as $\phi_0=0.55$. Figure 1 (top panel) shows the folded light curve of the pulsar for energies above 100 MeV. The light curve has two distinct peaks and is well fit by a constant plus two gaussians centered at phases $\phi = 0.26$ and $\phi = 0.77$, with their means separated by 0.51 ± 0.01 in phase. The “pulsed fraction” (determined by integrating the contribution from the two gaussians) is energy dependent, as can be appreciated from Figure 1. It has an unusually low value of $\sim 26 \pm 2$ % for energies above 100 MeV, with the remaining $>70\%$ coming from the constant term. While the pulsed fraction does increase at higher energies, up to $\sim 45\%$ above 1.5 GeV, it is always less than 50%, regardless of the cuts chosen.

We identify the following intervals: first peak (FP): $0.105 < \phi < 0.405$, second peak (SP): $0.632 < \phi < 0.904$, bridge (BR): $0.459 < \phi < 0.597$, and off-peak (OP): $0.938 < \phi < 0.053$. The lower panels show the folded light curve in 5 different energy intervals: 0.1–0.3 GeV, 0.3–1 GeV, 1–3 GeV, >3 GeV, and > 5 GeV (dark histogram in the second panel).

2.3. Spectral Analysis

We performed the spectral analysis using data collected during the sky survey: 2008 August 4 to 2009 June 30 (MJD 54682–55013). While the LAT data taken during the commissioning period are adequate for timing analyses, several of the configuration settings may have had a modest effect on the energy resolution and reconstruction, so we exclude these data for the spectral analysis. We also

exclude events with zenith angles greater than 105° to minimize the contamination from gamma rays from the Earth’s atmosphere. A phase-averaged spectrum was obtained with an unbinned maximum likelihood analysis, using the LAT Science Tool `gtlike` (Abdo et al. 2009b) and the “Pass 6 v3” instrument response functions (IRFs). We used energies > 200 MeV. The diffuse emission from the Milky Way was modeled using `gll_iem_v02`¹ while the isotropic extragalactic diffuse emission and residual instrumental particle backgrounds were modeled together using the currently recommended “template spectrum” `isotropic_iem_v02`¹. We extracted photons from a 15° radius ROI centered on the coordinates of RX J1836.2+5925, in order to properly account for the contributions of other gamma-ray sources in the vicinity. All sources from the LAT first-year source catalog (Abdo et al. 2010) included in our ROI were fit with a simple power law, while for the pulsar itself we used a power law with an exponential cutoff:

$$\frac{dN}{dE} = K E_{\text{GeV}}^{-\Gamma} \exp \left[- \left(\frac{E}{E_{\text{cutoff}}} \right)^n \right] \quad (1)$$

where Γ is the photon index, E_{cutoff} the cutoff energy, and K the normalization (in units of $\text{ph cm}^{-2} \text{s}^{-1} \text{MeV}^{-1}$). A super-exponential cutoff ($n = 2$) was ruled out, compared to a simple exponential ($n = 1$) cutoff, at 8σ significance so we set n equal to 1 in further analysis. Note that physical motivation for the use of a power-law spectrum with an exponential cutoff is underpinned by this being approximately the form expected for curvature or synchrotron radiation from both monoenergetic electrons (e.g. see Eq. (24) of Harding et al. 2008), and electrons with a distribution of Lorentz factors up to some maximum value. A superexponential cutoff, on the other hand, would be expected in polar cap models, due to single photon pair production attenuation in strong magnetic fields near the surface (Nel & de Jager 1995; Daugherty & Harding 1996; Razzano & Harding 2007). The results of our spectral fits are summarized in Table 2. The quoted errors are statistical only. The effect of the systematic uncertainties in the effective area on the spectral parameters is $\delta\Gamma = (+0.3, -0.1)$, $\delta E_{\text{cutoff}} = (+20\%, -10\%)$, $\delta F_{100} = (+30\%, -10\%)$, and $\delta G_{100} = (+20\%, -10\%)$ (Abdo et al. 2009f).

Next, we studied the energy spectrum in the various phase intervals defined in Section 2.2. The spectral parameters of the pulsar were allowed to be free, while those of the other sources were fixed to the values obtained in the phase-averaged analysis. Figure 2 shows the four spectra and Table 2 summarizes the results, normalized for the different phase intervals, pointing to mild variations of the photon index Γ and cutoff energy E_{cutoff} over the four phase intervals, with the off-peak region characterized by a softer spectrum. We also carried out a phase-resolved spectral analysis by taking 15 equal-counts bins of ~ 650 photons. As in the previous analysis, the parameters of all the sources in the ROI were fixed at the values obtained in the phase-averaged analysis. Figure 3 shows the results of our analysis. The top panel illustrates the evolution of the cutoff energy, while the bottom panel shows the change in photon index with phase. Insufficient photon statistics prevent us from investigating the apparent spectral changes within the peaks in any finer detail.

2.4. Variability analysis

2.4.1. Pulse profile variability

We checked for variability in the pulse profile shape using non parametric tests. First, the data were divided into time segments with equal counts (from 2 up to 32 segments). For every pair of segments, light curves were compared against the null hypothesis that both were drawn from the same parent distribution by performing Kolmogorov-Smirnov tests. There was no instance in which the pairwise comparison resulted in the null hypothesis being rejected even at the 80% confidence level. χ^2 tests yielded the same results, resulting in an overall gaussian distribution for the normalized residuals. We repeated the tests for light curves with 8, 10, 12, 15, 20, and 30 bins, confirming in every case that there is no hint of variability on timescales longer than a week.

2.4.2. Flux variability

In order to check the long term stability of the source, we computed the 0.1–100 GeV photon flux in 5-day time bins using the LAT Science Tool `gtlike`. First, we constructed a spectral model file including all the LAT first-year catalog point sources catalog (Abdo et al. 2010) in our ROI, the Galactic diffuse emission and the isotropic background. Since AGN in the region of interest can be variable, the spectral parameters of all point sources were set free while the Galactic and isotropic background were fixed to the values obtained in the first phase-averaged analysis. After running `gtlike`, we checked the fit result for sources with large uncertainties. After removing these sources with low significance ($< 2\sigma$), we ran `gtlike` again to obtain the flux of PSR J1836+5925 for that 5-day bin. Figure 4 shows the resulting fluxes and statistical uncertainties. We used five-day bins as this was the interval chosen by Bulgarelli et al. (2008), facilitating the comparison with the AGILE results. Assuming a constant flux, a χ^2 test gives a value of 66.2 with 65 degrees of freedom. The variability index of McLaughlin et al. (1996) is $V = 0.37$, consistent with no variation. The weighted standard deviation of the flux is 16% of the average. If the flux is assumed to change linearly with time, the slope is consistent with zero, with a 68% limit of 6.8% change from beginning to end of the data. Fitting a sinusoidal variation produces an amplitude of $(2.5 \pm 3.9)\%$ of the mean flux, consistent with zero. We note that while the overall flux seen by the LAT agrees with that reported by the EGRET experiment (Hartman et al. 1999), it is somewhat higher than what has been reported by the AGILE experiment (Bulgarelli et al. 2008; Pittori et al. 2009).

3. Multi-wavelength Analysis

3.1. Radio search

We used the LAT ephemeris to search anew for radio pulsations from PSR J1836+5925. We folded the 24 hr dataset obtained at the GBT in 2002 December (for details, see Halpern et al. 2007) modulo the predicted period, while searching in dispersion measure up to $DM = 100 \text{ cm}^{-3} \text{ pc}$, using PRESTO (Ransom 2001). For the distance range 250–800 pc (Halpern et al. 2007), the DM predicted by the NE2001 electron density model (Cordes & Lazio 2002) is $2\text{--}9 \text{ cm}^{-3} \text{ pc}$. Although there is no evidence in the LAT 2008–2009 timing solution for rotational instabilities, and we do not expect a large degree of timing noise from such a relatively old pulsar, we also did a small search in period about the nominal value. No radio pulsations were detected. For an assumed pulsar duty cycle of 10%, our long observation at a frequency of 0.8 GHz yields a flux density of $S_{0.8} < 7 \mu\text{Jy}$ (this is a significant improvement over the limit presented in Halpern et al. (2007) for the same data because we are now searching for a known period, allowing for a lower signal-to-noise ratio detection threshold). Converted to the more usual pulsar search frequency of 1.4 GHz with a typical spectral index of -1.6 , $S_{1.4} < 3 \mu\text{Jy}$. The implied luminosity is $L_{1.4} \equiv S_{1.4} d^2 < 0.002 d_{0.8}^2 \text{ mJy kpc}^2$. This is at least an order of magnitude smaller than the least luminous radio pulsar, PSR J1741–2054, originally discovered in gamma rays by the LAT (see Camilo et al. 2009), suggesting that if PSR J1836+5925 is an active radio pulsar its beam probably does not intersect the Earth. One caveat to this conclusion is that scintillation caused by the interstellar medium could be quite significant for this observation of this pulsar: depending on its actual DM within the expected range, the characteristic scintillation bandwidth and timescale at 0.8 GHz predicted by the NE2001 model may be greater than the observation bandwidth and time. If so, the received flux density of the pulsar during the observation may not reflect its intrinsic average. To address this potential concern, we did one extra observation with the GBT. On 2009 October 24 we recorded data from a bandwidth of 100 MHz centered on 350 MHz for 2.0 hr using GUPPI². Again, no pulsations were detected from PSR J1836+5925. For the same assumed duty cycle, the flux limit was $55 \mu\text{Jy}$. With the same assumed spectral index, this corresponds to $14 \mu\text{Jy}$ at 0.8 GHz. While this recent 350 MHz observation was thus nominally only half as sensitive as the earlier 24 hr observation at 820 MHz, it was still an extremely deep observation, and much more immune to scintillation effects, rendering our earlier conclusion valid: for all practical purposes, PSR J1836+5925 is a “radio quiet” pulsar.

3.2. X-ray observations

We studied the X-ray counterpart of PSR J1836+5925 using two *XMM-Newton* observations taken on 2008 May 18 and 2008 June 25 (15 ks each). Both the EPIC/pn (Strüder et al. 2001) and the EPIC/MOS (Turner et al. 2001) cameras were operated in their Full Frame mode, using the

²<https://wikio.nrao.edu/bin/view/CICADA/GUPPIUsersGuide>

thin optical filter. We focused on spectroscopy (the time resolution is not adequate to search for pulsations). Data reduction and analysis were performed with the *XMM-Newton* Science Analysis Software (SASv8.0). Owing to the lack of variability between the two epochs, the two data sets were merged, resulting in 24.4 ks, 30.7 ks and 30.8 ks of good exposure in the pn, MOS1 and MOS2 cameras, respectively. The background-subtracted 0.2–3 keV count rate of the source, as extracted from a 15'' radius circle, is 0.023 ± 0.001 cts s⁻¹, 0.0043 ± 0.0004 cts s⁻¹, and 0.0040 ± 0.0004 cts s⁻¹ in the pn, MOS1 and MOS2 cameras, respectively. Background accounts for $\sim 30\%$ additional counts.

We performed simultaneous fits to the pn, MOS1 and MOS2 spectra using the XSPEC v12.4 software. The X-ray spectrum cannot be described by a pure blackbody model ($\chi^2_\nu = 3.70$, 40 d.o.f.). A simple power law is possibly consistent with the data ($\chi^2_\nu = 1.39$, 40 d.o.f.), however, the best fit requires a rather large photon index ($\Gamma = 3.0 \pm 0.2$) and a very low N_H of $< 2 \times 10^{19}$ cm⁻² (errors are at 90% confidence level for a single parameter).

The combination of a blackbody and a power law yields a better fit ($\chi^2_\nu = 0.71$, 38 d.o.f.). The best fit model features an absorbing column $N_H < 2.7 \times 10^{20}$ cm⁻² (the best fit value is 0), a blackbody temperature³ $kT = 59^{+7}_{-17}$ eV, and a power law photon index $\Gamma = 1.7 \pm 0.3$. The total observed flux in 0.2–5 keV is 5.5×10^{-14} erg cm⁻² s⁻¹. Table 3 summarizes the results of our best spectral fit.

While our flux values are not dissimilar from those of Halpern et al. (2002), the black-body temperature, as well as the N_H values can now be constrained directly on the basis of the *XMM* data.

The rather high value of the blackbody temperature, coupled with the very low N_H (consistent with 0) point to a small emitting surface at a relatively low distance. For the best fitting temperature, an emitting surface of 1 km radius would imply a 450 pc distance which would scale to 300 pc for a 50 eV temperature. In no way can emission from the entire neutron star be invoked since it would imply a distance in excess of 3 kpc, not compatible with our very low N_H . In such a scenario the contribution of the thermal emission from the bulk of the surface should be negligible within the EPIC band. This requires⁴ a surface temperature lower than ~ 25 eV (~ 30 eV), assuming a 10 km emitting radius at 300 pc (450 pc), which is consistent with expectations for a $\sim 10^6$ yr old neutron star. Such a cooler thermal component would also be consistent with the deep HST upper limits.

The overall similarity of the X-ray spectrum of PSR J1836+5925 and Geminga is apparent in Figure 5, where both the *XMM* spectra and curves fitting the phase-averaged LAT spectra

³We quote blackbody temperatures and emitting radii as measured by a distant observer throughout the paper.

⁴In order to get a rough estimate, we fixed all spectral parameters of the blackbody plus powerlaw model to their best fitting values, leaving N_H as a free parameter (with a maximum allowed value of 2.7×10^{20} cm⁻²), and we added a second blackbody component to account for surface emission.

for both these sources are depicted. This similarity applies to both the X-ray and γ -ray spectra individually, to the LAT-band turnovers, to the offset between their fluxes in each waveband, and therefore to the overall multiwavelength impression (for the detailed LAT results on Geminga, see Abdo et al. 2009e). This broadband picture clearly illustrates that PSR J1836+5925 resembles Geminga in its high energy components, a character that will guide future spectral modeling. The extrapolation of the *XMM* power law tails up to the LAT band highlights the disparity between the X-ray non-thermal indices $\Gamma \sim 1.7$ and the LAT band power law indices $\Gamma \sim 1.3$. This property suggests that some as yet undetectable spectral structure or feature must exist in the 20 keV – 100 MeV band, perhaps due to a transition between components spawned by different radiative processes. The structure may be a simple flattening, or something more complex, however it should be unlike the steepening seen in the broadband X-ray/ γ -ray spectrum of the younger Vela pulsar (Strickman et al. 1999). The diagnostic potential enabled by the detection of such spectral structure motivates the development of future sensitive spectroscopy telescopes in the hard X-ray and soft γ -ray bands.

We also re-analyzed archival *Chandra* data taken in high time resolution, to search for possible X-ray pulsations. Using 118 ks of HRC-S data (the same dataset described by Halpern et al. 2007), we extracted ~ 790 source counts. No significant modulation is apparent in a 10 bin phase histogram folding the events with the extrapolated LAT timing solution. Although we expect no significant timing noise from this pulsar, a search for pulsations was also performed around a narrow range of the expected period (0.1732–0.1733 s), but no significant signal was detected. Following Vaughan et al. (1994), we set an upper limit of 40% on the pulsed fraction (at 99% confidence level), assuming a sinusoidal modulation.

4. Discussion

The discovery by the LAT of PSR J1836+5925 confirmed the long-held suspicion that 3EG J1835+5918 was a nearby Geminga-like pulsar. Its characteristic age of 1.8 million years agrees with expectations that it should be significantly older than Geminga, given the soft X-ray spectrum of its X-ray counterpart, the absence of optical and radio emission, and the measured upper limits on its proper motion (Halpern et al. 2007). We see no evidence for time variability of either the source flux or the pulse profile shape over the 11 months of observations. Our measured pulsations explain why this pulsar proved rather difficult to detect: the small ($\sim 30\%$) pulse fraction and relatively large duty cycle made blind searches of EGRET data futile. Indeed, it necessitated the LAT pointed observations to get an early pulse detection. Our detection, in turn, raises several puzzles – why does this object have such a large off-peak component and how does the relatively low spindown power produce an apparently large γ -ray luminosity for even modest distances?

While other pulsars show detectable emission throughout most of the pulsar period (e.g. see Abdo et al. 2009b,d), that of PSR J1836+5925 is particularly bright, and provides a good opportunity to test the nature of these off-peak components. Since the source at pulse minimum is

unresolved, and since the pulse minimum spectrum demands a 2–3 GeV cutoff, we conclude that we are not seeing evidence for a surrounding pulsar wind nebula (PWN). The lack of extended emission in the deep *Chandra* images also implies that there is no bright PWN. Thus the off-peak flux is likely magnetospheric. Since the $\Gamma \approx 1.6$ off-peak spectral index is substantially softer than that of the rest of the profile, we tested whether a second, spatially unresolved pulsar could contribute the off-peak flux. We searched for pulsations from the source by applying the standard time-differencing technique (Atwood et al. 2006), masking the frequency of PSR J1836+5925. We used a maximum frequency of 64 Hz, and a long time-difference window of ~ 12 days. We found no evidence for pulsations at any other frequency. The precise sensitivity of the blind search is still not completely understood, however, a comparison of the blind search pulsars discovered so far (Abdo et al. 2009a) and the known radio pulsars detected by the LAT, suggests that the blind search is approximately 2–3 times less sensitive than a standard pulsation search using the known timing solution (Abdo et al. 2009f). This results in a 5σ limit on the pulsed flux of $\sim 2 \times 10^{-7} \text{ cm}^{-2} \text{ s}^{-1}$ for another putative pulsar at this location. We conclude that PSR J1836+5925 emits over half its flux in a nearly constant component with an exponentially cut-off spectrum which is softer than the peaks of the profile.

The distance inferred from the observed γ -ray flux, $F_\gamma = 6 \times 10^{-10} \text{ erg cm}^{-2} \text{ s}^{-1}$, depends on the intrinsic luminosity (L_γ), the beam geometry, and the line of sight along which we sample the anisotropic emission. To account for anisotropy, we parameterize the relation between the observed flux and the true luminosity by the “flux conversion factor” $f_\Omega = L_\gamma/4\pi d^2 F_\gamma$, whose estimation we discuss in the next paragraph. The intrinsic luminosity can be inferred from the spindown luminosity of the pulsar, if we know the efficiency $\eta = L_\gamma/\dot{E}$. We therefore have $d = (\dot{E}/4\pi F_\gamma)^{1/2}(\eta/f_\Omega)^{1/2}$. It has been argued that the efficiency of γ -ray emission, and the fraction of the open zone participating in the gaps, grows with decreasing \dot{E} (Ruderman & Cheng 1988; Arons 1996), and observations support $\eta \propto \dot{E}^{-1/2}$ (Abdo et al. 2009f). We adopt $\eta = C(\dot{E}/10^{33} \text{ erg s}^{-1})^{-1/2}$, where C is a slowly varying function of order unity which depends on the details of the physical model (Watters et al. 2009). The observed $\dot{E} = 1.1 \times 10^{34} \text{ erg s}^{-1}$ then implies an efficiency of $\eta \sim 0.30$. Using this efficiency, along with the known values for γ -ray flux F_γ and spindown luminosity \dot{E} , our estimate for the pulsar distance becomes $d \approx 215 f_\Omega^{-1/2} \text{ pc}$.

The factor f_Ω depends sensitively on the emission model, on the inclination of the pulsar spin axis to the line of sight (ζ), and on the inclination of the magnetic pole with respect to the spin axis (α). Models are described in Watters et al. (2009); for the “Two Pole Caustic” (TPC) model, pulse separations $\Delta = 0.5$ occur in two regions: $\alpha \gtrsim 85^\circ$, $\zeta \lesssim 60^\circ$ or $\alpha \lesssim 60^\circ$, $\zeta \gtrsim 85^\circ$ (near the axes in the magenta zone of Figure 3 in Watters et al. 2009). The former solutions are, however, not satisfactory as they have weak bridge fluxes, at least for models with thin radiating surfaces. Thicker emission zones can produce additional bridge flux (Venter et al. 2009). The large ζ solutions can indeed have substantial off-peak flux arising at modest $r < 0.2 r_{LC}$ altitudes (where $r_{LC} = cP/2\pi$ is the speed of light cylinder), especially for efficiencies $\eta \lesssim 0.2$. For the outer gap (OG) model, only a few $\zeta \gtrsim 80^\circ$, $\alpha \lesssim 30^\circ$ models give the observed Δ for highly efficient pulsars ($\eta \sim 0.2$).

These have relatively large off-peak fluxes, arising from large $r > 0.5 r_{LC}$ altitudes.

While both models have acceptable large ζ solutions, for the TPC model the f_Ω is typically 0.9 ± 0.1 , with the small α solutions trending to $f_\Omega > 2$. In contrast, the few acceptable OG models have $f_\Omega \lesssim 0.1$. The resulting distance for the TPC model is typically $d \approx 250$ pc (but in some cases can be $d \lesssim 170$ pc). For the OG model we expect $d \approx 750$ pc. Both cases are small enough to be compatible with the small X-ray absorption discussed in Section 3.2. In summary, the TPC model has more acceptable solutions, but would imply a very small distance. The relatively small parameter space of acceptable OG solutions, on the other hand, is offset by a larger source distance and hence a larger Galaxy volume in which such a pulsar could be found.

In general, the results of our X-ray analyses are in broad agreement with previous investigations (Halpern et al. 2002), which were based on a factor > 3 smaller photon statistics. Our analysis clearly shows that the spectrum of the candidate counterpart is indeed consistent with the one of a nearby, thermally-emitting, middle-aged isolated neutron star.

The best prospect for refining our understanding of the emission from PSR J1836+5925 would clearly come from an accurate distance measurement. This seems difficult to obtain, although improved X-ray spectral measurements and models could help. Alternatively, if γ -ray pulsar spectral models can be developed sufficiently, we may be able to connect the softer off-peak spectrum with a particular magnetospheric location. In either case, the low power, large characteristic age and relatively close distance imply that J1836+5925 is the harbinger of a large population of old and weak γ -ray pulsars (Abdo et al. 2009a,c).

The *Fermi* LAT Collaboration acknowledges generous ongoing support from a number of agencies and institutes that have supported both the development and the operation of the LAT as well as scientific data analysis. These include the National Aeronautics and Space Administration and the Department of Energy in the United States, the Commissariat à l’Energie Atomique and the Centre National de la Recherche Scientifique / Institut National de Physique Nucléaire et de Physique des Particules in France, the Agenzia Spaziale Italiana and the Istituto Nazionale di Fisica Nucleare in Italy, the Ministry of Education, Culture, Sports, Science and Technology (MEXT), High Energy Accelerator Research Organization (KEK) and Japan Aerospace Exploration Agency (JAXA) in Japan, and the K. A. Wallenberg Foundation, the Swedish Research Council and the Swedish National Space Board in Sweden.

Additional support for science analysis during the operations phase is gratefully acknowledged from the Istituto Nazionale di Astrofisica in Italy and the Centre National d’Études Spatiales in France.

The GBT is operated by the National Radio Astronomy Observatory, a facility of the National Science Foundation operated under cooperative agreement by Associated Universities, Inc.

This work is partly based on observations obtained with *XMM – Newton*, an ESA science

mission with instruments and contributions directly funded by ESA Member States and NASA.

REFERENCES

- Abdo, A. A. et al. 2009a, *Science*, 325, 840
- . 2009b, *ApJ*, 696, 1084
- . 2009c, *ApJ*, in preparation (Eight γ -ray pulsars discovered in blind frequency searches of Fermi LAT data)
- . 2009d, *ApJ*, submitted (Fermi LAT Observations of the Crab Pulsar and Nebula)
- . 2009e, *ApJ*, in preparation (Fermi LAT observations of the Geminga pulsar)
- . 2009f, *ApJ*, submitted (The First Fermi Large Area Telescope Catalog of Gamma-ray Pulsars), [arXiv:0910.1608](#)
- . 2010, *ApJ*, to be Submitted (Fermi Large Area Telescope First Source Catalog)
- Arons, J. 1996, *A&AS*, 120, C49
- Atwood, W. B. et al. 2009, *ApJ*, 697, 1071
- Atwood, W. B., Ziegler, M., Johnson, R. P., & Baughman, B. M. 2006, *ApJ*, 652, L49
- Bignami, G. F., & Caraveo, P. A. 1996, *ARA&A*, 34, 331
- Bulgarelli, A. et al. 2008, *A&A*, 489, L17
- Camilo, F. et al. 2009, *ApJ*, 705, 1
- Caraveo, P. A., Bignami, G. F., DeLuca, A., Mereghetti, S., Pellizzoni, A., Mignani, R., Tur, A., & Becker, W. 2003, *Science*, 301, 1345
- Chandler, A. M., Koh, D. T., Lamb, R. C., Macomb, D. J., Mattox, J. R., Prince, T. A., & Ray, P. S. 2001, *ApJ*, 556, 59
- Cordes, J. M., & Lazio, T. J. W. 2002, [arXiv: astro-ph/0207156](#)
- Daugherty, J. K., & Harding, A. K. 1996, *ApJ*, 458, 278
- Fegan, S. J., & Weekes, T. C. 2005, *Ap&SS*, 297, 431
- Halpern, J. P., Camilo, F., & Gotthelf, E. V. 2007, *ApJ*, 668, 1154
- Halpern, J. P., Gotthelf, E. V., Mirabal, N., & Camilo, F. 2002, *ApJ*, 573, L41

- Halpern, J. P., & Ruderman, M. 1993, *ApJ*, 415, 286
- Harding, A. K., Stern, J. V., Dyks, J., & Frackowiak, M. 2008, *ApJ*, 680, 1378
- Hartman, R. C. et al. 1999, *ApJS*, 123, 79
- Hobbs, G. B., Edwards, R. T., & Manchester, R. N. 2006, *MNRAS*, 369, 655
- Lin, Y. C. et al. 1992, *IAU Circ.*, 5676, 2
- McLaughlin, M. A., Mattox, J. R., Cordes, J. M., & Thompson, D. J. 1996, *ApJ*, 473, 763
- Mirabal, N., & Halpern, J. P. 2001, *ApJ*, 547, L137
- Mirabal, N., Halpern, J. P., Eracleous, M., & Becker, R. H. 2000, *ApJ*, 541, 180
- Nel, H. I., & de Jager, O. C. 1995, *Ap&SS*, 230, 299
- Nolan, P. L. et al. 1996, *ApJ*, 459, 100
- Pittori, C. et al. 2009, *A&A*, in press
- Ransom, S. M. 2001, *Harvard University*, 93, 216
- Ray, P. S. et al. 2010, *ApJ*, in preparation (Precise Timing of Gamma-ray Pulsars with the Fermi LAT)
- Razzano, M., & Harding, A. K. 2007, in *American Institute of Physics Conference Series*, Vol. 921, The First GLAST Symposium, ed. S. Ritz, P. Michelson, & C. A. Meegan, 413–414
- Reimer, O., Brazier, K. T. S., Carramiñana, A., Kanbach, G., Nolan, P. L., & Thompson, D. J. 2000, in *American Institute of Physics Conference Series*, Vol. 510, American Institute of Physics Conference Series, ed. M. L. McConnell & J. M. Ryan, 489–493
- Reimer, O., Brazier, K. T. S., Carramiñana, A., Kanbach, G., Nolan, P. L., & Thompson, D. J. 2001, *MNRAS*, 324, 772
- Ruderman, M., & Cheng, K. S. 1988, *ApJ*, 335, 306
- Strickman, M. S., Harding, A. K., & de Jager, O. C. 1999, *ApJ*, 524, 373
- Strüder, L. et al. 2001, *A&A*, 365, L18
- Totani, T., Kawasaki, W., & Kawai, N. 2002, *PASJ*, 54, L45
- Turner, M. J. L. et al. 2001, *A&A*, 365, L27
- Vaughan, B. A. et al. 1994, *ApJ*, 435, 362

- Venter, C., Harding, A. K., & Guillemot, L. 2009, ApJ, submitted, arXiv: 0911.0872 (Probing Millisecond Pulsar Emission Geometry using Light Curves from the Fermi-LAT)
- Watters, K. P., Romani, R. W., Weltevrede, P., & Johnston, S. 2009, ApJ, 695, 1289
- Ziegler, M., Baughman, B. M., Johnson, R. P., & Atwood, W. B. 2008, ApJ, 680, 620

Table 1: Measured and derived timing parameters for PSR J1836+5925

Parameter	Value ^a
MJD range	54647.4–55013.0
Epoch (MJD)	54800
R.A. (J2000)	18:36:13.75(3)
Dec. (J2000)	+59:25:30.3(6)
ν (Hz)	5.7715514983(4)
$\dot{\nu}$ (Hz s ^{−1})	$-4.97(2) \times 10^{-14}$
Rms timing residual (ms)	1.3
Characteristic age, τ_c (kyr)	1840
\dot{E} (erg s ^{−1})	1.1×10^{34}
Surface magnetic dipole field strength (gauss)	5.1×10^{11}
γ -ray peak separation (Δ)	0.51 ± 0.01

^aThe numbers in parentheses are the 1σ uncertainties derived from the timing model (see Section 2.1).

Table 2: LAT γ -ray spectral results PSR J1836+5925

Phase region ^a	Parameter	Value ^b
	MJD range	54682.7–55013.0
Phase-averaged $0 < \phi < 1$	Photon Flux, F_{100} (ph cm ⁻² s ⁻¹)	$(6.24 \pm 0.12) \times 10^{-7}$
	Energy Flux, G_{100} (erg cm ⁻² s ⁻¹)	$(5.91 \pm 0.08) \times 10^{-10}$
	Photon Index, Γ	1.31 ± 0.03
	Cutoff Energy, E_{cutoff} (GeV)	2.27 ± 0.11
	Normalization, K (ph cm ⁻² s ⁻¹ MeV ⁻¹)	$(1.82 \pm 0.06) \times 10^{-10}$
First Peak (FP) $0.105 < \phi < 0.405$	Photon Flux, F_{100} (ph cm ⁻² s ⁻¹)	$(8.32 \pm 0.24) \times 10^{-7}$
	Energy Flux, G_{100} (erg cm ⁻² s ⁻¹)	$(7.97 \pm 0.17) \times 10^{-10}$
	Photon Index, Γ	1.31 ± 0.05
	Cutoff Energy, E_{cutoff} (GeV)	2.31 ± 0.17
	Normalization, K (ph cm ⁻² s ⁻¹ MeV ⁻¹)	$(2.42 \pm 0.12) \times 10^{-10}$
Second Peak (SP) $0.632 < \phi < 0.904$	Photon Flux, F_{100} (ph cm ⁻² s ⁻¹)	$(6.44 \pm 0.22) \times 10^{-7}$
	Energy Flux, G_{100} (erg cm ⁻² s ⁻¹)	$(6.40 \pm 0.16) \times 10^{-10}$
	Photon Index, Γ	1.24 ± 0.05
	Cutoff Energy, E_{cutoff} (GeV)	2.18 ± 0.18
	Normalization, K (ph cm ⁻² s ⁻¹ MeV ⁻¹)	$(2.03 \pm 0.12) \times 10^{-10}$
Bridge (BR) $0.459 < \phi < 0.597$	Photon Flux, F_{100} (ph cm ⁻² s ⁻¹)	$(4.47 \pm 0.28) \times 10^{-7}$
	Energy Flux, G_{100} (erg cm ⁻² s ⁻¹)	$(4.09 \pm 0.17) \times 10^{-10}$
	Photon Index, Γ	1.17 ± 0.11
	Cutoff Energy, E_{cutoff} (GeV)	1.64 ± 0.23
	Normalization, K (ph cm ⁻² s ⁻¹ MeV ⁻¹)	$(1.66 \pm 0.20) \times 10^{-10}$
Off-Peak (OP) $0.053 > \phi > 0.938$	Photon Flux, F_{100} (ph cm ⁻² s ⁻¹)	$(4.87 \pm 0.38) \times 10^{-7}$
	Energy Flux, G_{100} (erg cm ⁻² s ⁻¹)	$(3.63 \pm 0.19) \times 10^{-10}$
	Photon Index, Γ	1.59 ± 0.11
	Cutoff Energy, E_{cutoff} (GeV)	2.65 ± 0.57
	Normalization, K (ph cm ⁻² s ⁻¹ MeV ⁻¹)	$(9.90 \pm 1.2) \times 10^{-11}$

^aSee the top panel in Figure 1 for a visual representation of the various phase regions.

^bAll errors quoted are statistical. In addition, systematic errors of $\delta F_{100} = (+30\%, -10\%)$, $\delta G_{100} = (+20\%, -10\%)$, $\delta \Gamma = (+0.3, -0.1)$, and $\delta E_{\text{cutoff}} = (+20\%, -10\%)$ must be taken into account (Abdo et al. 2009f).

Table 3: Radio and X-ray results for PSR J1836+5925

Wavelength	Parameter	Value
Radio	Radio flux density at 350 MHz, $S_{0.35}(\mu\text{Jy})$	< 55
	Radio flux density at 0.8 GHz, $S_{0.8}(\mu\text{Jy})$	< 7
	Radio flux density at 1.4 GHz, $S_{1.4}(\mu\text{Jy})$ ^a	< 3
X-ray	(0.2–5 keV) Total observed ^b X-ray flux ($\text{erg cm}^{-2} \text{ s}^{-1}$)	5.5×10^{-14}
	(0.2–5 keV) Unabsorbed non-thermal flux ($\text{erg cm}^{-2} \text{ s}^{-1}$)	3.0×10^{-14}
	X-ray blackbody temperature, kT (eV)	59^{+7}_{-17}
	X-ray blackbody radius (km)	$(1.5^{+5.3}_{-0.4})d_{0.8}$ ^c
	X-ray absorbing column, N_H (cm^{-2})	$< 2.7 \times 10^{20}$
	X-ray power law photon index, Γ	1.7 ± 0.3
	X-ray power law normalization at 1 keV, N_{PL} ($\text{ph cm}^{-2} \text{ s}^{-1} \text{ keV}^{-1}$)	$(5.7 \pm 1.0) \times 10^{-6}$

^aThere is no measured upper limit at 1.4 GHz. This limit is derived from the observation made at 0.8 GHz (See Section 3.1)

^bTotal observed and unabsorbed flux coincide since the best fitting column density is $N_H=0$.

^c $d_{0.8}$ is the distance to PSR J1836+5925 in units of 0.8 kpc.

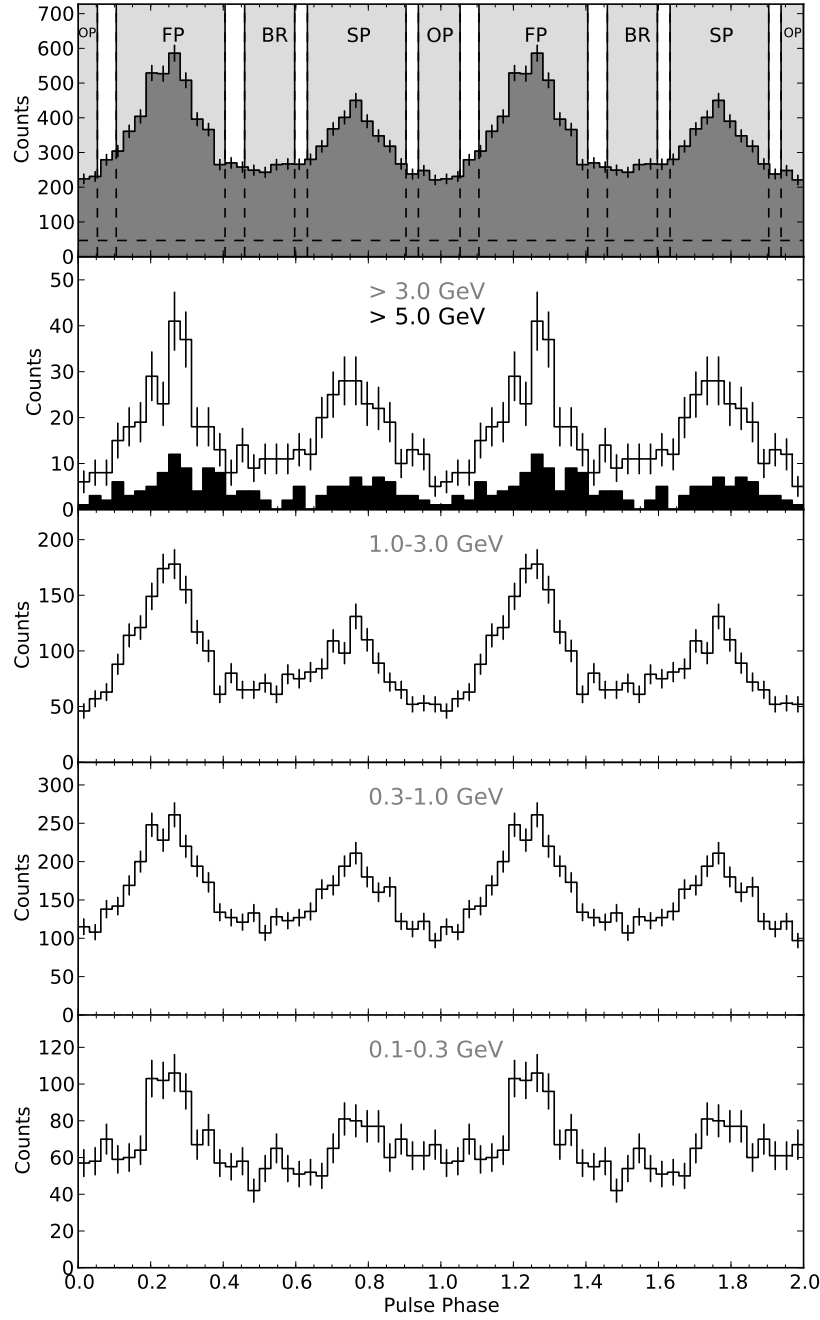


Fig. 1.— Folded light curves of PSR J1836+5925 with a resolution of 32 phase bins per period. Two rotations are shown. The top panel shows all events >100 MeV, along with the different phase regions labelled: Off-peak (OP), First Peak (FP), Bridge (BR), and Second Peak (SP) regions. The horizontal dashed line represents an estimate of the background due to diffuse emission, illustrating the high level of off-peak emission being emitted by the source. The lower four panels show the light curves in different energy bands. The darker histogram on the second panel from the top shows events with $E > 5$ GeV.

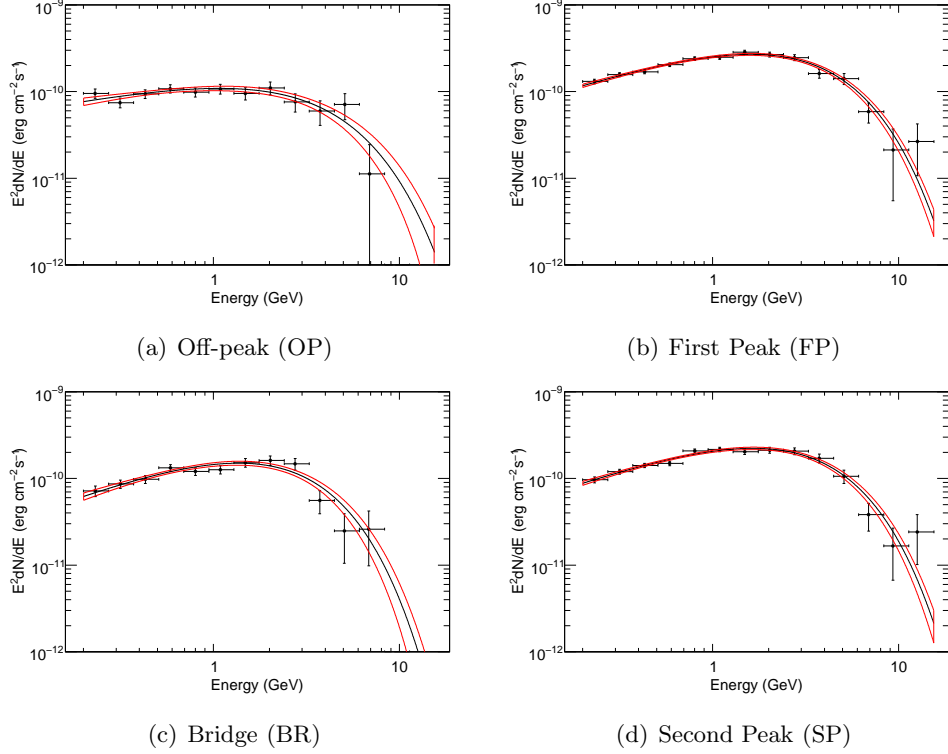


Fig. 2.— Energy spectra of the four identified phase regions of PSR J1836+5925. The data points represent the measured fluxes obtained from likelihood fits in different representative energy bands where the pulsar is modeled as a power law, while the line shows the best-fit model obtained in the unbinned maximum likelihood analysis over the entire energy range, along with the 1σ “bowtie” confidence region. **Top Left** – Off-peak (OP). **Top Right** – First Peak (FP). **Bottom Left** – Bridge (BR). **Bottom Right** – Second Peak (SP).

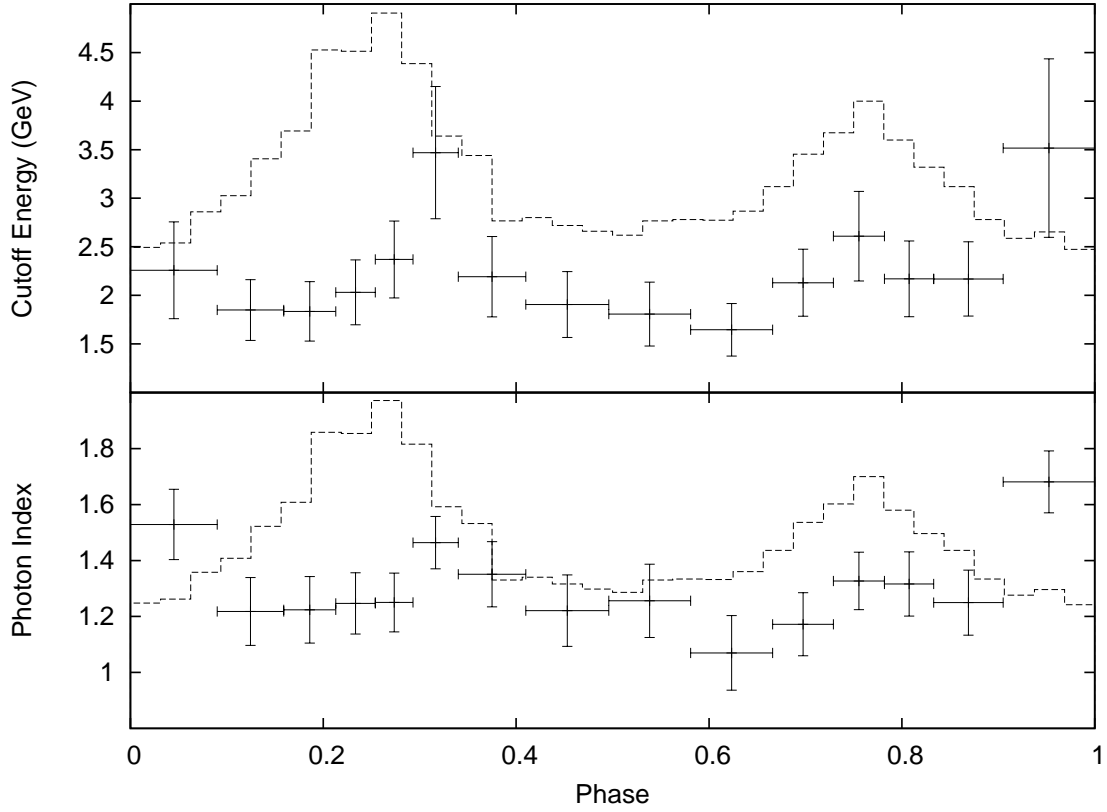


Fig. 3.— Cutoff energy (top) and photon index (bottom) as a function of phase for PSR J1836+5925 using 15 equal-count bins containing ~ 650 events each. The dashed line in both panels shows the >100 MeV folded light curve of PSR J1836+5925.

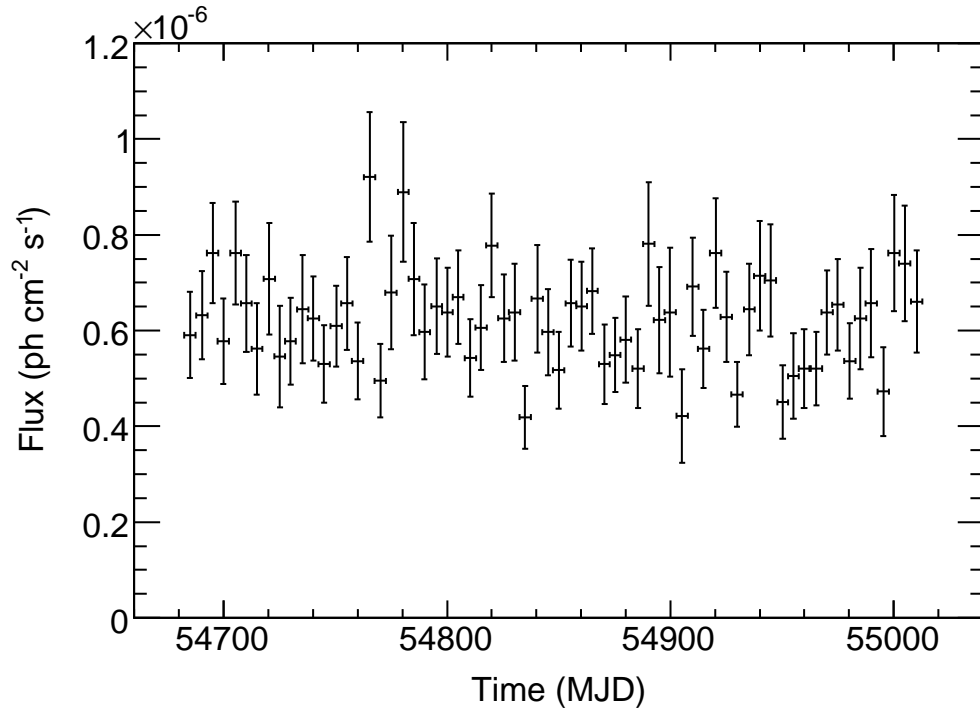


Fig. 4.— Flux of PSR J1836+5925 as a function of time in 5-day time bins, showing no evidence for variability (see Section 2.4.2).

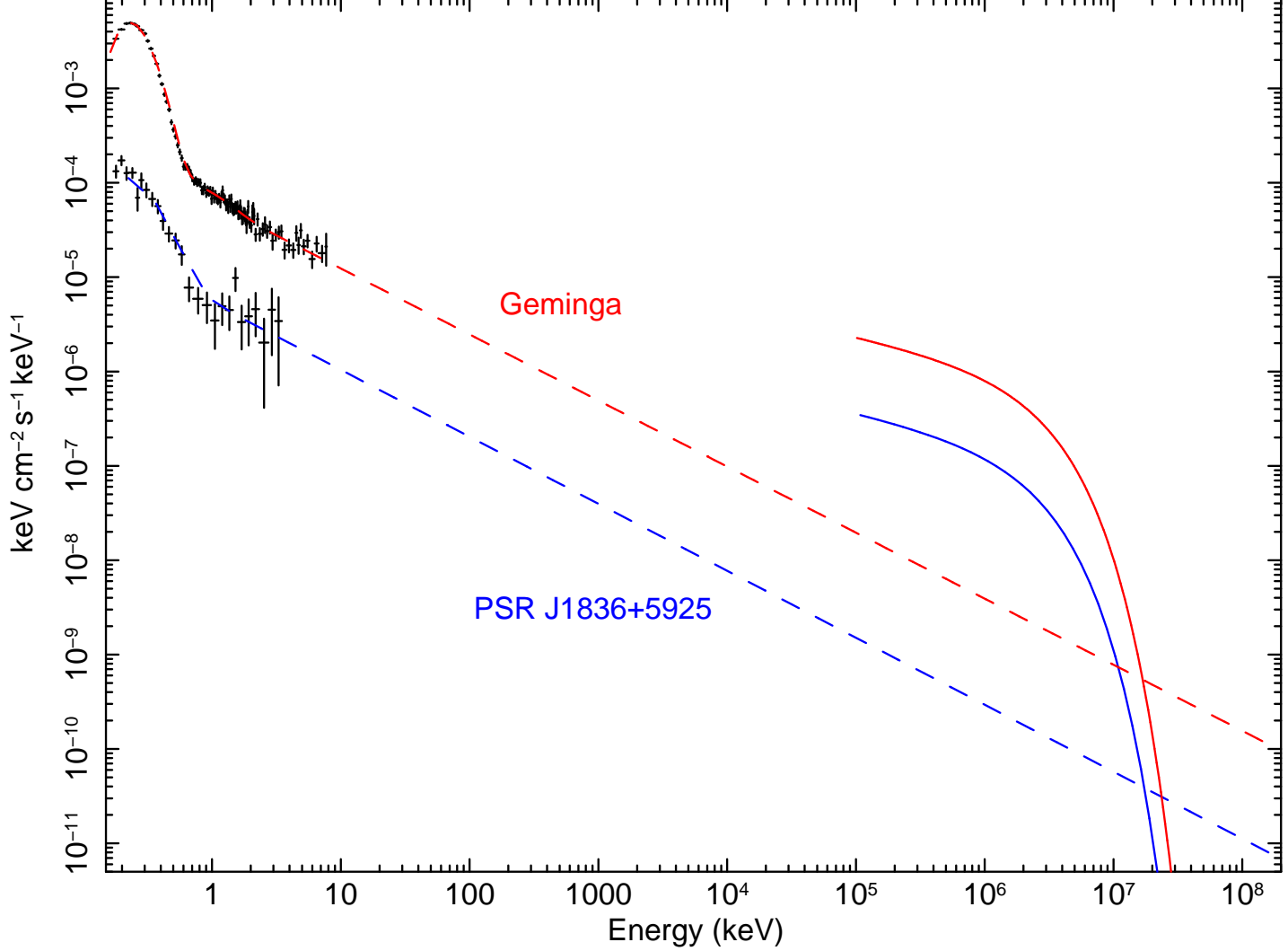


Fig. 5.— Unfolded *XMM-Newton* spectrum of PSR J1836+5925, compared to that of Geminga, whose data have been reprocessed to take advantage of the new calibration files which cover the energy range down to 0.15 keV (EPIC status of calibration and data analysis Document XMM-SOC-CAL-TN-0018 <http://xmm2.esac.esa.int/docs/documents/CAL-TN-0018.pdf>). The best fit models are superimposed (for a thorough report on Geminga, see Caraveo et al. 2003). We extrapolate the models out to the LAT energy range and show the best-fit phase-averaged LAT spectra for the two pulsars. The overall similarity is apparent.